THE JOURNAL OF PHYSICAL CHEMISTRY C

Article

pubs.acs.org/JPCC

CO Adsorption on the "29" Cu_xO/Cu(111) Surface: An Integrated DFT, STM, and TPD Study

Alyssa J. R. Hensley,[†] Andrew J. Therrien,[∥] Renqin Zhang,[†] Matthew D. Marcinkowski,[∥] Felicia R. Lucci,[∥] E. Charles H. Sykes,*[,∥] and Jean-Sabin McEwen*[,†,‡,§]

[†]The Gene and Linda Voiland School of Chemical Engineering and Bioengineering, [‡]Department of Physics and Astronomy, and [§]Department of Chemistry, Washington State University, Pullman, Washington 99164, United States

[∥]Department of Chemistry, Tufts University, Medford, Massachusetts 02155, United States

Supporting Information

ABSTRACT: The elucidation of an accurate atomistic model of surface structures is crucial for the design and understanding of effective catalysts, a process requiring a close collaboration between experimental observations and theoretical models. Any developed surface theoretical model must agree with experimental results for the surface when both clean and adsorbate covered. Here, we present a detailed study of the adsorption of CO on the "29" Cu_xO/Cu(111) surface, which is important in the understanding of ubiquitous Cu-based catalysis. This study uses scanning tunneling microscopy, temperature-programmed desorption, and density functional theory to analyze CO adsorption on the "29" Cu_xO/Cu(111) surface. From the experimental scanning tunneling microscopy images, CO was found to form six different ordered structures on the "29" Cu_xO/Cu(111) surface depending on the surface CO coverage. By modeling the adsorption of CO on our atomistic model of the "29" Cu_xO/Cu(111) surface at different coverages, we were able to match the experimentally observed CO ordered structures to specific combinations of sites on the "29" Cu_xO/Cu(111) surface. The high degree of agreement seen here between experiment and theory for the adsorption of CO on the "29" Cu_xO/Cu(111) surface at various CO coverages provides further support that our atomistic model of the "29" Cu_xO/Cu(111) surface is experimentally accurate.

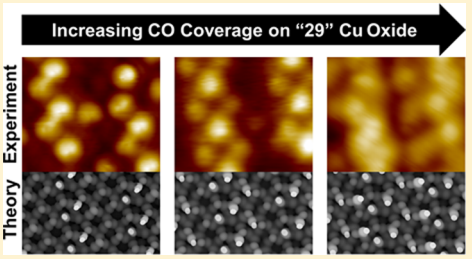

1. INTRODUCTION

Cu_xO catalysts have been shown to be an important class of catalysts for a number of reactions, including CO oxidation,[1−5] methanol synthesis,[6−9] partial oxidation of methanol,[10−12] methanol reforming,[13] and low-temperature water-gas shift.[14,15] The wide applicability of this class of catalyst is likely due to the ability of Cu to alternate between the Cu^0, Cu^+, and Cu^{2+} oxidation states, as pure metallic Cu cannot survive under redox conditions.[16] The reactivity of Cu is closely linked to its oxidation state; for example, CO adsorption is stronger on Cu^+ than Cu^{2+}, making the CO oxidation reaction more likely to occur when the Cu_xO surface is designed to contain a majority of Cu^+.[17] The active site for many of the listed industrial reactions is still debated, as even at low O chemical potentials Cu can form surface oxides. Additionally, these Cu_xO surfaces can be used as catalytic supports for other metal catalysts, similar to that seen for other metal oxides.[18−24] However, in order to improve the activity and selectivity of such Cu_xO catalysts, the catalyst structure and active sites require identification and characterization. Such insight into the atomistic structure of catalytic surfaces can only be obtained through a thorough and combined experimental and theoretical approach.

One Cu_xO surface of particular interest is the "29" Cu_xO/Cu(111) surface, which forms in ultrahigh vacuum (UHV) from the exposure of Cu(111) to a surface saturation dose of O_2 at ∼673 K.[25−27] This structure has long-range uniformity and is formed from a single layer of hexagonal Cu_2O rings atop the Cu(111) surface, with the rings distorting in order for the oxide to match the underlying (111) lattice.[28−32] The creation of an accurate model of the "29" Cu_xO/Cu(111) surface has been elusive due to the size and complexity of the "29" Cu_xO/Cu(111) unit cell, which has a unit cell 29 times larger than that of Cu(111), giving rise to its name. Until recently, the "29" Cu_xO/Cu(111) surface was modeled using reduced supercells that did not accurately reproduce the surface O density or capture the distortion of the Cu_2O rings.[28−32] In our previous work, we developed a promising atomistic model of the "29" Cu_xO/Cu(111) surface, capturing both the correct surface O density and surface corrugation.[33] The improved accuracy of our atomistic model of the "29" Cu_xO/Cu(111) surface was shown by a comparison of experimental and theoretical scanning tunneling microscopy (STM) images of the clean "29" Cu_xO/Cu(111) surface.[33] To confirm the accuracy of our proposed model of the "29" Cu_xO/Cu(111) surface, it is crucial to show that this theoretical model reproduces the adsorptive behavior observed experimentally for the "29" Cu_xO/Cu(111) surface.

Received: July 29, 2016
Revised: September 29, 2016
Published: October 4, 2016

DOI: 10.1021/acs.jpcc.6b07670
J. Phys. Chem. C 2016, 120, 25387−25394

Here, we examine the adsorption of CO on the "29" Cu_xO/Cu(111) surface via temperature-programmed desorption (TPD), STM, and density functional theory (DFT) simulations. This work fills a knowledge gap in the adsorption of CO on different Cu_xO surfaces. Previous studies for CO adsorption on several Cu_xO surfaces have shown that under sufficiently high CO pressures, the oxide surface reduces.[4,28] In order to maintain the ordered structure of the "29" Cu_xO/Cu(111) surface and quantitatively compare the experimental and theoretical results, we examined lower CO pressures here. The DFT simulations utilized the model "29" Cu_xO/Cu(111) surface developed in our previous work.[33] By comparing the experimental TPD and STM images to the DFT results for varying CO coverages on the "29" Cu_xO/Cu(111) surface, we were able to identify combinations of CO adsorption sites on our model of the "29" Cu_xO/Cu(111) surface which accurately reproduced the observed ordered structures. The high degree of agreement between theoretical and experimental results for the adsorption of CO on the "29" Cu_xO/Cu(111) surface indicates that our proposed atomistic model for this surface is experimentally accurate.

2. EXPERIMENTAL AND COMPUTATIONAL METHODS

2.1. Temperature-Programmed Desorption. TPD experiments were carried out in an UHV chamber with a base pressure of $<1 \times 10^{-10}$ mbar. The chamber was equipped with a quadrupole mass spectrometer (Hiden) where the Cu(111) crystal was able to be cooled to 85 K with liquid nitrogen and resistively heated to 750 K. The Cu(111) crystal was cleaned by Ar^+ sputtering and annealing to 750 K. The "29" oxide film was formed by exposure to O_2 gas (Airgas, USP grade) at a pressure of 5×10^{-6} mbar for 3 min at a sample temperature 650 ± 20 K. High precision leak valves allowed for accurate exposure of CO (Airgas, 99.99%). TPD measurements of CO were performed with a linear heating ramp of 1 K s^{-1} while monitoring m/z 28.

2.2. Scanning Tunneling Microscopy. For STM experiments the oxide film was prepared in a preparation chamber ($P = 2 \times 10^{-10}$ mbar) following the same protocol as in the TPD experiments. The sample was then transferred in UHV to the STM chamber ($P = 1 \times 10^{-11}$ mbar) and into the precooled 5 K STM stage. CO was deposited onto the 5 K surface using line-of-sight molecular dosers installed on the STM chamber. The sample was then annealed to 60 ± 20 K and cooled back to 5 K before imaging was conducted using a low-temperature Omicron NanoTechnology STM. Images were acquired using an etched W tip. Quoted scanning biases are with respect to the sample.

2.3. Density Functional Theory. The DFT calculations performed here utilized the Vienna *Ab Initio* Simulation Package (VASP) code,[34,35] where the core electrons were treated with the projector augmented wave (PAW) method.[36,37] The valence electrons for all systems were described using the generalized gradient approximation (GGA) with the Perdew–Burke–Ernzerhof (PBE) functional.[38] After identifying the best fitting CO adsorption configurations on the "29" Cu_xO/Cu(111) surface, these configurations were then re-examined using the vdW-DF functional,[39] which has been shown to reproduce the experimental adsorption energy for CO on Co(0001),[40] and the resulting adsorption energies are reported for both functionals. The optimized structures for CO on the "29" Cu_xO/Cu(111) surface obtained using the vdW-DF functional were identical to those obtained using the PBE functional.

All surface calculations were performed using a $(1 \times 2 \times 1)$ Monkhorst–Pack[41] **k**-points mesh. The energy cutoff for the plane wave basis set was set to 500 eV, and the electron smearing was described by the Methfessel–Paxton[42] smearing method with a width of 0.2 eV. Each calculation was considered converged when the total energy changed by less than 10^{-6} eV, and the forces between atoms were smaller than 0.02 eV/Å. The computational STM images were generated by using the constant current model, which is implemented in the p4vasp program using the Tersoff–Hamann approach.[43,44]

The "29" Cu_xO/Cu(111) surface (see Figure 1) was constructed by placing single a Cu_xO layer atop a four-layer

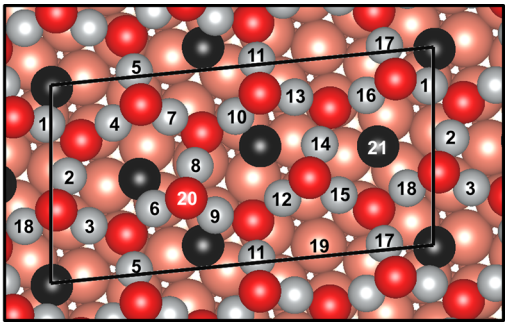

Figure 1. Top view of the model "29" Cu_xO/Cu(111) surface with the possible CO adsorption sites labeled numerically from 1 to 21. The pink, silver, red, and black spheres represent Cu in the Cu(111) surface, Cu in the Cu_xO layer, O in the Cu_xO layer, and O adatoms on the Cu(111) surface, respectively.

Cu(111) surface with a supercell size of $\sqrt{13}R46.1° \times 7R21.8°$, where the bottom two Cu(111) layers were kept fixed in their bulk positions. The Cu_xO layer is made from six fused hexagonal rings, each containing six Cu and six O atoms. Additionally, O adatoms are placed in either fcc or hcp sites in the centers of five of the six hexagonal rings. Further details for the model structure of the "29" Cu_xO/Cu(111) surface can be found in our previous publication.[33] The vacuum thickness used for the surface calculations was ~12 Å, and the optimum Cu lattice constant was calculated to be 3.635 Å with the PBE functional and 3.705 Å with the vdW-DF functional.

Here, we describe the nomenclature for the CO adsorption sites on the "29" Cu_xO/Cu(111) surface. The 21 possible adsorption sites for CO on the "29" Cu_xO/Cu(111) surface are labeled as 1–21, as shown in Figure 1. These numbers are used to reference where on the "29" Cu_xO/Cu(111) surface multiple CO molecules adsorb. For two, three, and four CO systems, the tested CO adsorption sites are designated as (a, b), (a, b, c), and (a, b, c, d), respectively, where a, b, c, and d denote the different CO adsorption site labeled in Figure 1. As an example, the adsorption of two CO molecules within the "29" Cu_xO/Cu(111) supercell at sites 4 and 18 is denoted by (4, 18). The adsorption energy for CO on the "29" Cu_xO/Cu(111) surface was calculated via

$$E_{ads} = \frac{E_{CO/S} - E_S - N_{CO}E_{CO}}{N_{CO}} \quad (1)$$

where $E_{CO/S}$, E_S, and E_{CO} are the total energies for the adsorbed CO systems, "29" Cu_xO/Cu(111) surface, and gas phase CO

DOI: 10.1021/acs.jpcc.6b07670
J. Phys. Chem. C 2016, 120, 25387–25394

molecule, and N_{CO} is the number of CO molecules adsorbing onto the "29" $Cu_xO/Cu(111)$ surface.

3. RESULTS AND DISCUSSION

3.1. Temperature-Programmed Desorption of CO on the "29" $Cu_xO/Cu(111)$ Surface. TPD experiments, shown in Figure 2, provide information regarding the binding energies

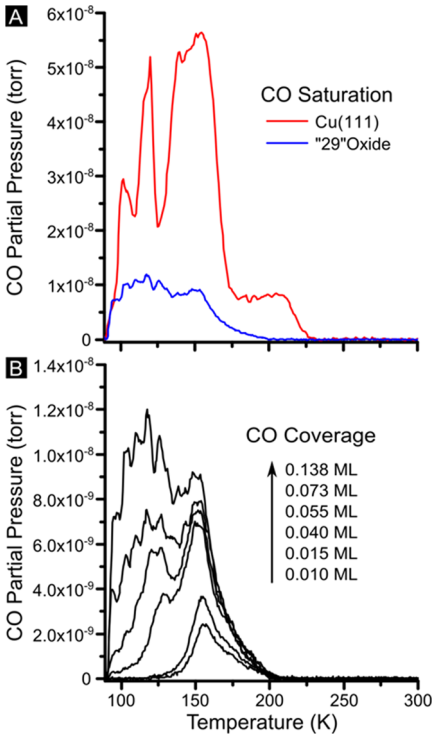

Figure 2. TPD traces monitoring the desorption of CO. (A) Desorption of saturation CO coverages on Cu(111) and the "29" oxide. (B) Family of TPD traces of different initial CO coverages on the "29" oxide, with coverages quoted with respect to the Cu(111) surface as discussed in the text.

and the structures of CO on the "29" oxide. The saturation coverage of CO on the oxide surface can be determined by comparison to the well-known CO/Cu(111) system. As shown in Figure 2A, the saturation coverage of CO on Cu(111) is much greater than the saturation coverage on the "29" oxide by nearly a factor of 4, determined by the area ratio. CO saturates on the Cu(111) surface at 0.52 ML with respect to the Cu(111) surface in which 1 ML is defined as 1.776×10^{15} atoms cm^{-2}, with the multiple peaks in the TPD trace attributed to the desorption of different CO packing structures and binding sites.[45−47] Thus, the saturation coverage of CO on the "29" oxide is determined to be 0.138 ML, with respect to Cu(111), which is equivalent to 4 CO molecules per unit cell of the "29" $Cu_xO/Cu(111)$ surface. One noteworthy observation is that the desorption temperature of CO from the two different systems is very similar. This generally means that the CO binding strength to metallic Cu and surface oxides of Cu is similar.

In Figure 2B, a family of TPD traces are shown leading up to the saturation coverage. At low coverage, a peak with a maximum at 154 K emerges and saturates just before the 0.040 ML trace. This corresponds to a preferred site on the oxide with one CO bound per unit cell of the "29" oxide. By Redhead analysis, the desorption barrier at this preferred site is 0.48 eV assuming a pre-exponential factor of 10^{15} s^{-1},[48] which is a common pre-exponential factor for adsorbates on oxide surfaces.[49] After this peak saturates, a broad lower temperature shoulder develops and grows with increased coverage. This low temperature peak is composed of three smaller peaks which, combined with the 154 K desorption feature, add up to the 4 CO's per oxide unit cell at saturation, shown in Figure S1. The presence of multiple peaks in the TPD spectra strongly indicates that several ordered structures could be present as one varies the CO coverage up to saturation.[50] To further investigate the interactions of CO on the oxide surface and the possible ordered structures at various CO coverages that are formed on the surface, STM experiments were performed at various CO exposures which revealed ordered structures that have been reproduced by DFT, further verifying the accuracy of the "29" $Cu_xO/Cu(111)$ model.[33]

3.2. Identification of Ordered CO Structures on the "29" $Cu_xO/Cu(111)$ Surface. *3.2.1. Low CO Coverage: One CO per Unit Cell.* Very low CO coverages on the "29" $Cu_xO/Cu(111)$ surface, at 1% of the saturation exposure, result in highly disperse features revealed by STM imaging, as shown in Figure 3a. These isolated protrusions are individual CO

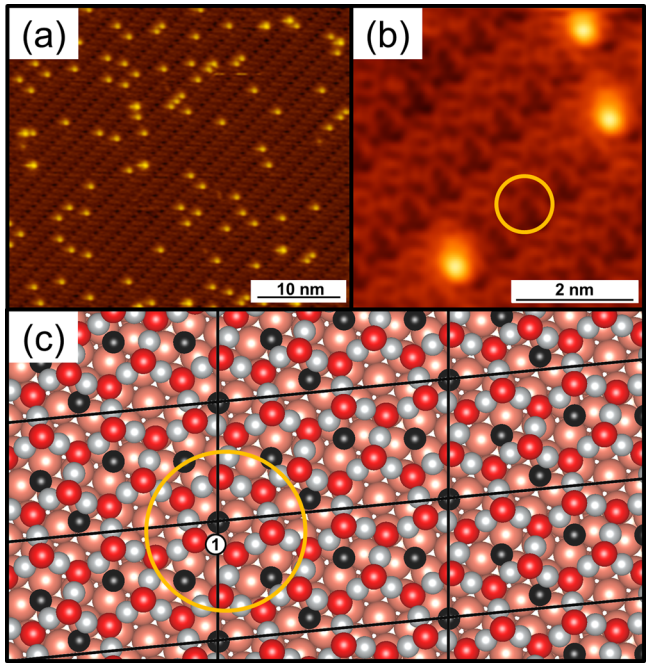

Figure 3. Experimental STM images of isolated CO molecules adsorbed onto the "29" $Cu_xO/Cu(111)$ surface at a bias of (a) 0.9 V and (b) 0.5 V. (c) The DFT model of the "29" $Cu_xO/Cu(111)$ surface with CO adsorption site 1 labeled. The yellow circle in (b) and (c) highlights a repeating dark feature of the oxide surface near which the isolated CO adsorb.

molecules. From the STM images, it is clear that these isolated CO adsorbates sit on the edge of the bright rows of the oxide. Furthermore, high-resolution STM imaging (Figure 3b) shows that the CO adsorbates (protrusions) are adjacent to a triangular patch of dark pores in the oxide.

In order to identify likely adsorption sites for the isolated CO adsorbates visualized in the experimental STM images, we examined the adsorption of one CO on the 21 different adsorption sites within one unit cell of our model "29" $Cu_xO/$

DOI: 10.1021/acs.jpcc.6b07670
J. Phys. Chem. C 2016, 120, 25387−25394

Cu(111) surface (Figure 1).[33] This corresponds to a CO coverage of 0.034 ML on the "29" Cu_xO/Cu(111) surface. The resulting adsorption energies for each tested site (see Table S1) show that the order of site preference is 8 > 9 > 1 > 10 > 13 > 18 > 4 > 15 > 17 > 6 > 3 > 16 > 14 > 19. The CO placed at sites 2, 5, 7, 11, 12, 20, and 21 desorbed from the "29" Cu_xO/Cu(111) surface and were therefore not considered in our following analyses.

Using DFT generated STM images of the clean "29" Cu_xO/Cu(111) surface,[33] the oxide features noted by the yellow circle in Figure 3b can be matched to specific rings in the model oxide structure (Figure 3c). Based on the calculated adsorption energies for an isolated CO molecule on these rings, this limits the possible CO adsorption sites observed in the low CO coverage experimental STM images to sites 1, 3, 4, 6, 8, 14, 17, and 18. The most stable of these possible, isolated CO adsorption sites is site 8. However, this site is discounted as the optimized structure for site 8 (Figure S2) shows that the adsorbed CO molecule in this site leans outside of the circle noted in Figure 3c. However, the second strongest binding site within the marked area for CO is site 1, which is centrally located in the circle and in the optimized structure CO remains relatively upright. The difference in the calculated binding energy between sites 1 and 8 is 0.06 eV, which is within DFT error, and along with other assumptions built into the DFT methods still makes for reasonable agreement between theory and experiment. Therefore, these results suggest that the isolated CO sites on the "29" Cu_xO/Cu(111) surface can be matched to CO molecules adsorbed at site 1.

3.2.2. Medium–Low CO Coverage: Two CO per Unit Cell. Imaging the CO covered "29" Cu_xO/Cu(111) surface at intermediate CO exposures of approximately 50% of saturation resulted in the appearance of three distinct CO ordered structures (Figure 4), which we name the "box", "zigzag", and "parallelogram" structures. The repetitive nature of these ordered structures suggests that these patterns result from the presence of 2 CO adsorbates per "29" Cu_xO/Cu(111) surface unit cell. Using the previously identified stable CO adsorption sites, 23 possible combinations of 2 CO sites per unit cell were modeled, all with a CO coverage of 0.069 ML. The resulting DFT simulated STM images were then compared to the experimental STM images of each ordered structure to determine the CO sites that account for the observed ordered structures. In addition to the visual comparison of the theoretical and experimental STM images, the distance between adsorbed CO species were measured by line scans between the CO protrusions (Table 1). These measurements were then compared to the CO–CO distances from the optimized DFT structures (Table 1 and Table S3). The STM images for all tested 2 CO per unit cell configurations are shown in Figures S4–S6, and the best fits for each ordered structure are shown in Figure 4.

The best fitting 2 CO per unit cell structures for each ordered structure were chosen based on the visual comparison of the DFT and experimental STM images as well as the DFT calculated CO–CO distances and angles (Table 1 and Table S3) matching to the experimentally determined range within ±1.5 Å and ±15°. First, for the box ordered structure, the (18, 10), (18, 8), (16, 8), and (1, 9) adsorption sites had the best fits. Second, for the zigzag ordered structure, the (4, 18), (16, 1), and (1, 14) had the best fits. Finally, for the parallelogram ordered structure, the (3, 10), (10, 1), and (9, 18) had the best fits.

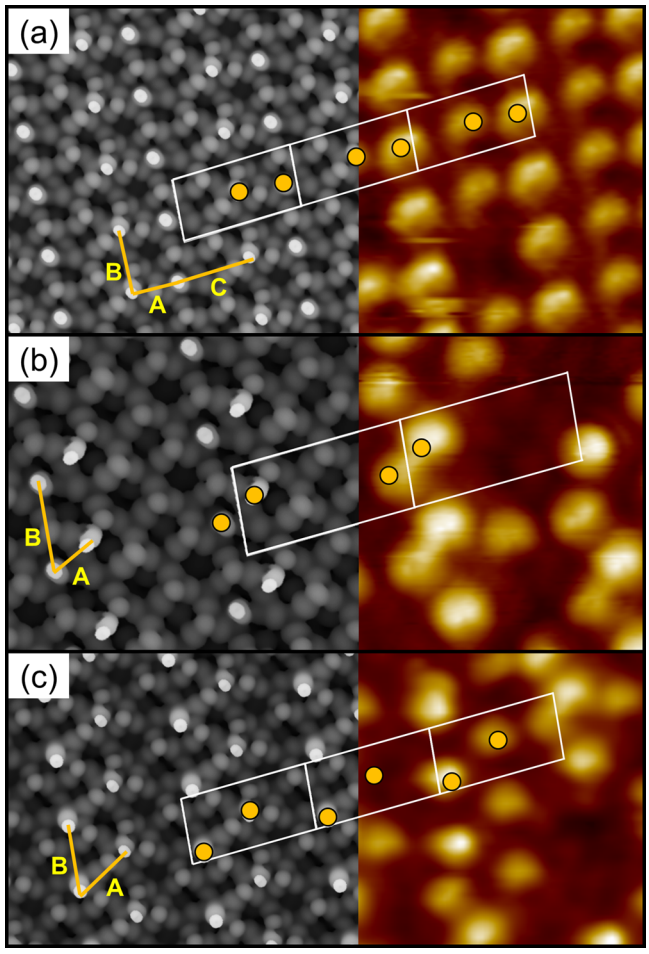

Figure 4. Experimental (right) and best fitting theoretical (left) DFT simulated STM images of CO adsorbed on the "29" Cu_xO/Cu(111) for the 2 CO/unit cell (a) box (18, 10), (b) zigzag (4, 18), and (c) parallelogram (3, 10) ordered structures. The imaging bias is 0.9 V for both experimental and theoretical STM images. The unit cell size (white box) is 9.27 Å by 17.99 Å in all images.

Based on the STM and geometric analysis of the 23 tested 2 CO per unit cell sites on the "29" Cu_xO/Cu(111) surface for each individual ordered structure, the possible sites were reduced to 10. Further analysis of the 2 CO per unit cell sites was possible using large scale experimental STM images (Figure 5) which showed that each of the three ordered structures have sites in common as the ordered structures were observed to have smooth transitions between the phases. For example, the dimmer CO site in the zigzag structure matches directly onto the bright CO site in the box structure. This additional constraint further limits the possible 2 CO per unit cell sites, arriving at one possible combination of sites being the (18, 10), (4, 18), and (3, 10) sites for the box, zigzag, and parallelogram ordered structures, where site 18 is the dim zigzag and bright box sites, 4 is the bright zigzag site, 3 is the bright parallelogram site, and 10 is the dim box and parallelogram sites. DFT simulated STM images of these most probable sites are those shown in Figure 4 next to their corresponding experimental STM images. Another interesting phenomenon observed in the 2 CO per unit cell structures is that none of the CO remains at site 1, the preferred adsorption site at low coverage, which reveals the dynamic nature of the adsorption process.

DOI: 10.1021/acs.jpcc.6b07670
J. Phys. Chem. C 2016, 120, 25387–25394

Table 1. Distances and Angles between Adsorbed CO Molecules on the "29" $Cu_xO/Cu(111)$ Surface for the 2 CO/Unit Cell and 3 CO/Unit Cell Ordered Structures Measured Both Experimentally and Theoretically (The Labels Reference Figures 4 and 6)

Experiment									
System	A (Å)	B (Å)	C (Å)	D (Å)	E (Å)	θ_1*,†	θ_2*,†	θ_3*,†	θ_4†,‡
Box	8.4±0.4	9.6±0.1	9.8±0.5	-	-	83±5	-	-	-
Zig-Zag	4.4±0.4	9.7±0.3	-	-	-	41±5	-	-	-
Parallelogram	8.4±0.3	9.4±0.4	-	-	-	58±5	-	-	-
Braid	7.0±0.4	9.4±0.1	11.2±0.4	5.9±0.3	5.4±0.6	83±5	35±5	47±5	75±5
Defect-Braid	19.0±0.4	-	7.0±0.4	9.0±0.4	10.0±0.4	67±5	32±5	-	-
Theory									
System	A (Å)	B (Å)	C (Å)	D (Å)	E (Å)	θ_1*,†	θ_2*,†	θ_3*,†	θ_4†,‡
Box	7.0	9.3	11.1	-	-	88	-	-	-
Zig-Zag	4.3	9.3	-	-	-	62	-	-	-
Parallelogram	8.3	9.3	-	-	-	58	-	-	-
Braid	10.4	9.3	10.0	6.7	4.7	84	61	24	78
Defect-Braid	19.4	-	6.4	11.4	10.7	78	47	-	-

[a]Angles for the box, zigzag, parallelogram, and braid structures are defined as $\theta_1 = \angle AB$, $\theta_2 = \angle BD$, and $\theta_3 = \angle AD$. Angles for the defect-braid structure are defined as $\theta_1 = \angle AD$ and $\theta_2 = \angle DE$ (see Figures 4 and 6). [b]All angles are in units of degrees. [c]The definition for θ_4 is shown in Figure 6a.

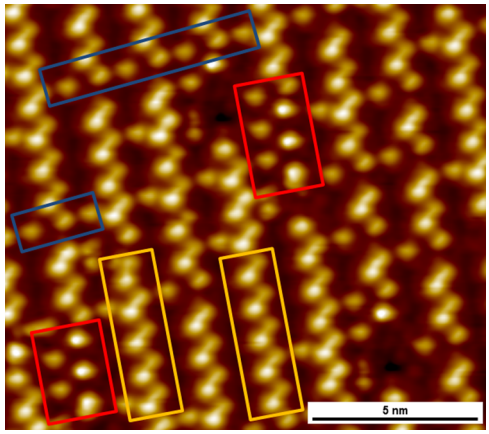

Figure 5. Experimental STM image of CO adsorbed on the "29" $Cu_xO/Cu(111)$ at intermediate CO exposure at a scanning bias of 0.9 V. The STM image shows how the three types of 2 CO/unit cell ordered structures merge: box (blue), zigzag (yellow), and parallelogram (red).

3.2.3. Medium–High CO Coverage: Three CO per Unit Cell. On the same surface as prepared experimentally with a 50% CO saturation exposure, some areas of the surface contained patches of 2 CO structures, while others contained 3 CO structures. An observed 3 CO structure is shown in Figure 6a. This ordered structure, referred to here as the "braid" structure, appears to be formed from the addition of a third CO molecule to the 2 CO per unit cell zigzag ordered structure. Increasing the number of CO molecules adsorbed onto the model "29" $Cu_xO/Cu(111)$ surface increases the modeled CO coverage to 0.103 ML. By matching the best fitting zigzag ordered structure, site (4, 18), to the 3 CO per unit cell braid structure, we were able to determine that there were three possible combinations that could account for the formation of the experimentally observed braid structure based on geometric matching: (4, 18, 6), (4, 18, 8), and (4, 18, 9). Additionally, the second best fitting 2 CO per unit cell zigzag ordered structure, site (1, 14), was fit to the 3 CO per unit cell braid structure, and the resulting possible structures were sites (1, 14, 9) and (1, 14, 10).

While the majority of the 3 CO per unit cell structures observed in the experimental STM images form the braid

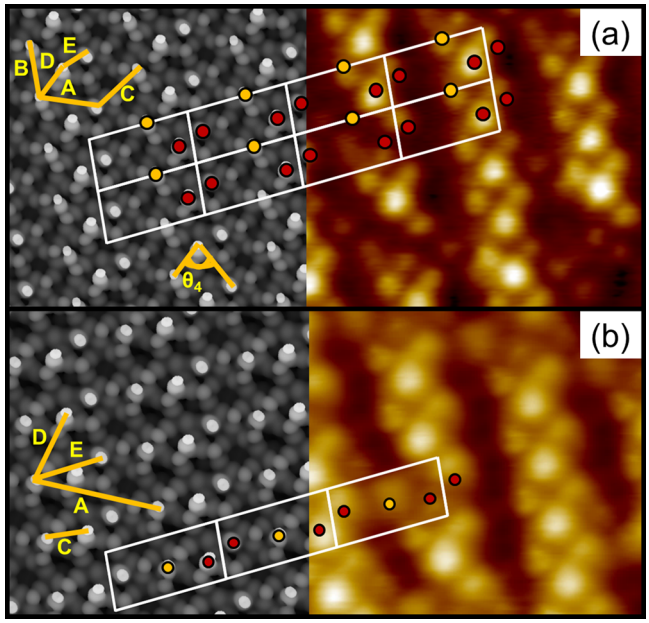

Figure 6. Experimental (right) and best fitting theoretical (left) DFT simulated STM images of CO adsorbed on the "29" $Cu_xO/Cu(111)$ for the 3 CO/unit cell. (a) The braid ordered structure (4, 18, 9), along with (b) the defect-braid structure (4, 18, 10) imaged at a sample bias of 0.9 V for both experimental and theoretical images. The unit cell size (white box) is 9.27 Å by 17.99 Å in all images. The red dots show the (4, 18) zigzag backbone structure.

structure (Figure 6a), there is a fairly consistent defect to this structure observed (Figure 6b). This defect is the result of the third CO of the braid structure moving to an adjacent binding site on the dark oxide rows where there is no CO, and this structure is denoted here as the "defect-braid". The site candidates for the defect-braid structure were, as before, determined by location matching the best and second best fitting 2 CO per unit cell zigzag sites. For the (4, 18) 2 CO per unit cell zigzag site, the possible defect-braid sites are (4, 18, 8), (4, 18, 10), (4, 18, 13), and (4, 18, 14). For the (1, 14) 2 CO per unit cell zigzag site, the possible defect-braid sites are (1, 14, 8) and (1, 14, 10).

The six possible candidates for each of the 3 CO per unit cell braid and defect-braid sites were compared to both the

DOI: 10.1021/acs.jpcc.6b07670
J. Phys. Chem. C 2016, 120, 25387−25394

experimental STM images and the line scan results (Table 1 and Table S4) for the CO−CO distances and CO−CO−CO angles in order to determine the best fit for both structures. STM images for all tested sites for the 3 CO per unit cell structures are shown in Figures S7 and S8. The best fitting 3 CO per unit cell site for the braid ordered structure was determined to be the (4, 18, 9) site, while the best fitting defect-braid structure was determined to be the (4, 18, 10) site. This matching is also consistent with the experimental STM evidence that 2 sites are fixed, 4 and 18 which make up the zigzag structure, and only the location of the third CO is moved to make the two different braid and defect-braid structures. The DFT generated simulated STM images for these 3 CO structures are shown in Figure 6.

3.2.4. High CO Coverage: Four CO per Unit Cell. Saturation of the "29" $Cu_xO/Cu(111)$ surface with CO was achieved by exposure to excess CO, resulting in a CO coverage of ∼0.138 ML along with the appearance of a new ordered structure (Figure 7). This structure originates from the braid

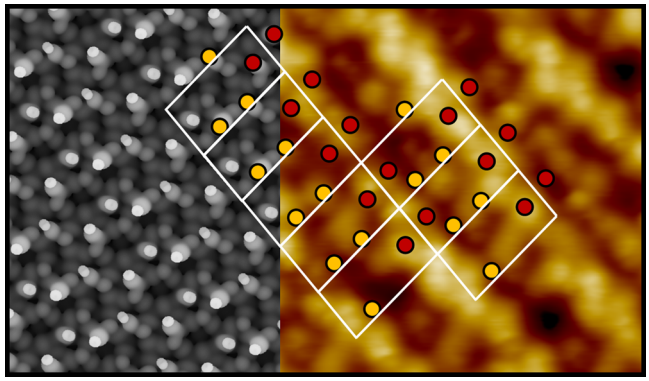

Figure 7. Experimental (right) and best fitting theoretical (left) DFT simulated STM images of CO adsorbed on the "29" $Cu_xO/Cu(111)$ for the 4 CO/unit cell ordered structure (4, 18, 9, 13). The STM bias is 0.9 V for both experimental and theoretical images. The unit cell size (white box) is 9.27 Å by 17.99 Å. The red dots show the (4, 18) zigzag backbone structure.

configuration observed for lower CO exposures (Figure 6a) by the addition of a fourth CO between the bright braid structure rows (theoretical CO coverage was 0.138 ML). Starting from the best fitting 3 CO per unit cell braid structure, site (4, 18, 9), the possible sites for this high coverage, 4 CO per unit cell structure were determined to be (4, 18, 9, 13), (4, 18, 9, 14), and (4, 18, 9, 17). STM images for all tested sites for the 4 CO per unit cell structures are shown in Figure S9. By comparing the DFT generated STM images for the possible 4 CO per unit cell sites with the experimental STM images, the optimal structure was determined to be the (4, 18, 9, 13) site (Figure 7).

3.3. CO Adsorption Energy Analysis. By comparing between DFT models and experimental STM images of CO adsorbed on the "29" $Cu_xO/Cu(111)$ surface, we were able to match the experimentally observed CO ordered structures at varying CO coverages to specific combinations of the 12 stable CO adsorption sites on our model of the "29" $Cu_xO/Cu(111)$ surface. The resulting adsorption energies for each of the structures matched to the experimental STM images were calculated and are shown in Table 2, along with the adsorption energies predicted from the Redhead analysis of the CO TPD on the "29" $Cu_xO/Cu(111)$ surface. The DFT calculated CO

Table 2. Average CO Adsorption Energies for the Four Different CO Coverages on the "29" $Cu_xO/Cu(111)$ Surface

		DFT E_{ads} (eV/CO)	
N_{CO}/unit cell	TPD E_{ads} (eV/CO)[a]	PBE	vdW-DF
1	−0.48	−0.89[b]	−0.68[b]
2	−0.45	−0.74/−0.77/−0.80[c]	−0.63/−0.64/−0.65[c]
3	−0.42	−0.76/−0.76[d]	−0.62/−0.66[d]
4	−0.39	−0.71[e]	−0.63[e]

[a]The adsorption energies from TPD are assumed to be the negative of the desorption barrier, as common for unactivated first-order desorption processes, which was calculated using the peak fits [Supporting Information] by a Redhead analysis assuming a pre-exponential factor of 10^{15} s^{-1}. [b]E_{ads} value corresponds to site 1. [c]E_{ads} values correspond to sites (4, 18)/(3, 10)/(18, 10), respectively. [d]E_{ads} values correspond to sites (4, 18, 10)/(4, 18, 9), respectively. [e]E_{ads} value corresponds to site (4, 18, 9, 13).

adsorption energies are significantly larger than the value predicted by the Redhead analysis of the experimental CO TPD on the "29" $Cu_xO/Cu(111)$ surface. This is consistent with the known overbinding errors of standard DFT methods.[51] Because of the overbinding, our comparisons of DFT and experimental adsorption energies will focus on the relative differences in the average adsorption energies with increasing CO coverage.

From both the Redhead and DFT analyses, it is clear that the average CO adsorption energy decreases as the number of CO per "29" $Cu_xO/Cu(111)$ unit cell increases. This decrease is ∼0.03 eV/CO from TPD and ∼0.06 eV/CO or ∼0.02 eV/CO from DFT using the PBE or vdW-DF functionals, respectively. Additionally, the 2, 3, and 4 CO structures per unit cell are all calculated to be very close in average CO binding strength from DFT. The flexibility of the underlying surface oxide structure plays an important role in such similar adsorption energies. Indeed, if one does not allow the surface oxide structure to relax as CO adsorbs, one finds that the CO molecule does not bind to the surface (Figure S10). As such, allowing the surface oxide to relax mitigates to a certain degree the repulsive lateral interactions between the CO molecules. Such interplay between the strain components of the adsorbate−adsorbate interactions and the electronic components of the lateral interactions were investigated to a certain degree for O[52,53] and CO[54] on single crystal metal surfaces, but seem to play a larger role for thin oxide films similar to those investigated here. As a result, the predicted desorption rates of the various structures are quite similar, which is consistent with the development of a broad low temperature shoulder in the CO uptake TPDs, as opposed to the evolution of well-separated desorption features for each of the structures that one would expect if large differences between the adsorption energies would be present. This high degree of agreement between theory and experiment concerning the adsorption of CO on the "29" $Cu_xO/Cu(111)$ surface, based on both the CO adsorption energy change with coverage and the evolution of ordered structures observed by STM, provides further evidence that we have developed an experimentally accurate, atomistic model of the "29" $Cu_xO/Cu(111)$ surface.

4. CONCLUSIONS

The adsorption of CO on the "29" $Cu_xO/Cu(111)$ surface was examined using a combination of experimental and theoretical

DOI: 10.1021/acs.jpcc.6b07670
J. Phys. Chem. C 2016, 120, 25387−25394

techniques. Comparing Cu(111) to the "29" surface oxide, it is clear that the CO binding strength to these surfaces is very similar, but the molecular density of CO at saturation is ~4 times lower on the oxide. The lower CO density on the surface can be directly attributed to fewer favorable CO binding sites on the "29" Cu_xO/Cu(111) surface. By extrapolation from this model study, a lower steady state coverage of CO under catalytic conditions on a Cu_xO catalysts would be expected relative to metallic Cu, which may be beneficial or detrimental to the catalytic conversion depending on the reaction. Furthermore, our model of the "29" Cu_xO/Cu(111) surface is validated by the agreement between experiment and theory. When exposed to different amounts of CO, six different ordered structures for CO on the "29" Cu_xO/Cu(111) surface were observed via experimental STM images, with surface coverages corresponding to 1, 2, 3, and 4 CO's per "29" Cu_xO/Cu(111) surface unit cell. By identifying the possible individual CO adsorption sites on our model of the "29" Cu_xO/Cu(111) surface, we were able to match each of the experimentally observed CO ordered structures to specific combinations of CO adsorption sites within the "29" Cu_xO/Cu(111) surface unit cell. Excellent agreement was found between experiment and theory when comparing STM and DFT simulated images, measured CO−CO distances and CO−CO−CO angles, and CO adsorption energies for each of the ordered structures. This high degree of agreement between the experimental and theoretical results for CO adsorbing on the "29" Cu_xO/Cu(111) surface provides further support that our atomistic model of the "29" Cu_xO/Cu(111) surface is experimentally accurate.

■ ASSOCIATED CONTENT

Supporting Information

The Supporting Information is available free of charge on the ACS Publications website at DOI: 10.1021/acs.jpcc.6b07670.

Peak fits to the CO saturation TPD on the "29" oxide, optimized structures of single CO sites on the "29" Cu_xO/Cu(111) surface; STM image comparisons between theory and experiment for all tested 2, 3, and 4 CO/unit cell sites; adsorption energies and structural parameters for all tested 2, 3, and 4 CO/unit cell sites (PDF)

■ AUTHOR INFORMATION

Corresponding Authors

*(J.-S.M.) Ph 509-335-8580, Fax 509-335-4806, e-mail js.mcewen@wsu.edu

*(E. C. H. S.) Ph 617-627-3773, Fax 617-627-3443, e-mail charles.sykes@tufts.edu.

Notes

The authors declare no competing financial interest.

■ ACKNOWLEDGMENTS

Financial support was provided by the National Science Foundation EAGER program under Contract CBET-1552320. The work at Tufts was supported by the Department of Energy BES under Grant DE-FG02-05ER15730. M.M. thanks Tufts Chemistry for an Illumina Fellowship. It was also partially funded by USDA/NIFA through Hatch Project #WNP00807 titled: "Fundamental and Applied Chemical and Biological Catalysts to Minimize Climate Change, Create a Sustainable Energy Future, and Provide a Safer Food Supply". A portion of the computer time for the computational work was performed using EMSL, a national scientific user facility sponsored by the Department of Energy's Office of Biological and Environmental Research and located at PNNL. PNNL is a multiprogram national laboratory operated for the U.S. DOE by Battelle.

■ REFERENCES

(1) Eren, B.; Lichtenstein, L.; Wu, C. H.; Bluhm, H.; Somorjai, G. A.; Salmeron, M. Reaction of CO with Preadsorbed Oxygen on Low-Index Copper Surfaces: An Ambient Pressure X-ray Photoelectron Spectroscopy and Scanning Tunneling Microscopy Study. *J. Phys. Chem. C* **2015**, *119*, 14669−14674.

(2) Domagala, M. E.; Campbell, C. T. The Mechanism of CO Oxidation over Cu(110): Effect of CO Gas Energy. *Catal. Lett.* **1991**, *9*, 65−70.

(3) Szanyi, J.; Goodman, D. W. CO Oxidation on a Cu(100) Catalyst. *Catal. Lett.* **1993**, *21*, 165−174.

(4) Yang, F.; Choi, Y.; Liu, P.; Hrbek, J.; Rodriguez, J. A. Autocatalytic Reduction of a Cu_2O/Cu(111) Surface by CO: STM, XPS, and DFT Studies. *J. Phys. Chem. C* **2010**, *114*, 17042−17050.

(5) Baber, A. E.; Xu, F.; Dvorak, F.; Mudiyanselage, K.; Soldemo, M.; Weissenrieder, J.; Senanayake, S. D.; Sadowski, J. T.; Rodriguez, J. A.; Matolín, V.; et al. In Situ Imaging of Cu_2O under Reducing Conditions: Formation of Metallic Fronts by Mass Transfer. *J. Am. Chem. Soc.* **2013**, *135*, 16781−16784.

(6) Klier, K. Methanol Synthesis. *Adv. Catal.* **1982**, *31*, 243−313.

(7) Chinchen, G. C.; Waugh, K. C.; Whan, D. A. The Activity and State of the Copper Surface in Methanol Synthesis Catalysts. *Appl. Catal.* **1986**, *25*, 101−107.

(8) Szanyi, J.; Goodman, D. W. Methanol Synthesis on a Cu(100) Catalyst. *Catal. Lett.* **1991**, *10*, 383−390.

(9) Behrens, M.; Studt, F.; Kasatkin, I.; Kühl, S.; Hävecker, M.; Abild-Pedersen, F.; Zander, S.; Girgsdies, F.; Kurr, P.; Kniep, B.-L.; et al. The Active Site of Methanol Synthesis over Cu/ZnO/Al_2O_3 Industrial Catalysts. *Science* **2012**, *336*, 893−897.

(10) Russell, J. N.; Gates, S. M.; Yates, J. T. Reaction of Methanol with Cu(111) and Cu(111) + O(ads). *Surf. Sci.* **1985**, *163*, 516−540.

(11) Boucher, M. B.; Marcinkowski, M. D.; Liriano, M. L.; Murphy, C. J.; Lewis, E. A.; Jewell, A. D.; Mattera, M. F. G.; Kyriakou, G.; Flytzani-Stephanopoulos, M.; Sykes, E. C. H. Molecular-Scale Perspective of Water-Catalyzed Methanol Dehydrogenation to Formaldehyde. *ACS Nano* **2013**, *7*, 6181−6187.

(12) Bluhm, H.; Hävecker, M.; Knop-Gericke, A.; Kleimenov, E.; Schlögl, R.; Teschner, D.; Bukhtiyarov, V. I.; Ogletree, D. F.; Salmeron, M. Methanol Oxidation on a Copper Catalyst Investigated Using in Situ X-Ray Photoelectron Spectroscopy. *J. Phys. Chem. B* **2004**, *108*, 14340−14347.

(13) Palo, D. R.; Dagle, R. A.; Holladay, J. D. Methanol Steam Reforming for Hydrogen Production. *Chem. Rev.* **2007**, *107*, 3992−4021.

(14) Newsome, D. S. The Water-Gas Shift Reaction. *Catal. Rev.: Sci. Eng.* **1980**, *21*, 275−318.

(15) Ovesen, C. V.; Stoltze, P.; Nørskov, J. K.; Campbell, C. T. A Kinetic Model of the Water Gas Shift Reaction. *J. Catal.* **1992**, *134*, 445−468.

(16) Hanson, J. C.; Si, R.; Xu, W.; Senanayake, S. D.; Mudiyanselage, K.; Stacchiola, D.; Rodriguez, J. A.; Zhao, H.; Beyer, K. A.; Jennings, G.; et al. Pulsed-Reactant *In Situ* Studies of Ceria/CuO Catalysts Using Simultaneous XRD, PDF and DRIFTS Measurements. *Catal. Today* **2014**, *229*, 64−71.

(17) Yang, B.-X.; Ye, L.-P.; Gu, H.-J.; Huang, J.-H.; Li, H.-Y.; Luo, Y. A density functional theory study of CO oxidation on CuO_{1-x}(111). *J. Mol. Model.* **2015**, *21*, 1−7.

(18) Ding, K.; Gulec, A.; Johnson, A. M.; Schweitzer, N. M.; Stucky, G. D.; Marks, L. D.; Stair, P. C. Identification of Active Sites in CO Oxidation and Water-Gas Shift over Supported Pt Catalysts. *Science* **2015**, *350*, 189−192.

DOI: 10.1021/acs.jpcc.6b07670
J. Phys. Chem. C 2016, 120, 25387−25394

(19) Zhou, X.; Yang, W.; Chen, Q.; Geng, Z.; Shao, X.; Li, J.; Wang, Y.; Dai, D.; Chen, W.; Xu, G.; et al. Stable Pt Single Atoms and Nanoclusters on Ultrathin CuO Film and Their Performances in CO Oxidation. *J. Phys. Chem. C* **2016**, *120*, 1709−1715.
(20) Dvorak, F.; Farnesi Camellone, M.; Tovt, A.; Tran, N. D.; Negreiros, F. R.; Vorokhta, M.; Skala, T.; Matolinova, I.; Myslivecek, J.; Matolin, V.; et al. Creating Single-Atom Pt-Ceria Catalysts by Surface Step Decoration. *Nat. Commun.* **2016**, *7*, 10801.
(21) Fu, Q.; Saltsburg, H.; Flytzani-Stephanopoulos, M. Active Nonmetallic Au and Pt Species on Ceria-Based Water-Gas Shift Catalysts. *Science* **2003**, *301*, 935−938.
(22) Qiao, B.; Wang, A.; Yang, X.; Allard, L. F.; Jiang, Z.; Cui, Y.; Liu, J.; Li, J.; Zhang, T. Single-atom catalysis of CO oxidation using Pt_1/FeO_x. *Nat. Chem.* **2011**, *3*, 634−641.
(23) Wang, Y.-G.; Mei, D.; Glezakou, V.-A.; Li, J.; Rousseau, R. Dynamic Formation of Single-Atom Catalytic Active Sites on Ceria-Supported Gold Nanoparticles. *Nat. Commun.* **2015**, *6*, 6511.
(24) Zhai, Y.; Pierre, D.; Si, R.; Deng, W.; Ferrin, P.; Nilekar, A. U.; Peng, G.; Herron, J. A.; Bell, D. C.; Saltsburg, H.; et al. Alkali-Stabilized Pt-OH_x Species Catalyze Low-Temperature Water-Gas Shift Reactions. *Science* **2010**, *329*, 1633−1636.
(25) Matsumoto, T.; Bennett, R. A.; Stone, P.; Yamada, T.; Domen, K.; Bowker, M. Scanning Tunneling Microscopy Studies of Oxygen Adsorption on Cu(111). *Surf. Sci.* **2001**, *471*, 225−245.
(26) Jensen, F.; Besenbacher, F.; Lægsgaard, E.; Stensgaard, I. Oxidation of Cu(111): Two New Oxygen Induced Reconstructions. *Surf. Sci.* **1991**, *259*, L774−L780.
(27) Jensen, F.; Besenbacher, F.; Stensgaard, I. Two New Oxygen Induced Reconstructions on Cu(111). *Surf. Sci.* **1992**, *269−270*, 400−404.
(28) An, W.; Baber, A. E.; Xu, F.; Soldemo, M.; Weissenrieder, J.; Stacchiola, D.; Liu, P. Mechanistic Study of CO Titration on Cu_xO/Cu(1 1 1) ($x \leq 2$) Surfaces. *ChemCatChem* **2014**, *6*, 2364−2372.
(29) An, W.; Xu, F.; Stacchiola, D.; Liu, P. Potassium-Induced Effect on the Structure and Chemical Activity of the Cu_xO/Cu(1 1 1) ($x \leq 2$) Surface: A Combined Scanning Tunneling Microscopy and Density Functional Theory Study. *ChemCatChem* **2015**, *7*, 3865−3872.
(30) Soon, A.; Todorova, M.; Delley, B.; Stampfl, C. Oxygen Adsorption and Stability of surface oxides on Cu(111): A First-Principles Investigation. *Phys. Rev. B: Condens. Matter Mater. Phys.* **2006**, *73*, 165424.
(31) Soon, A.; Todorova, M.; Delley, B.; Stampfl, C. Thermodynamic Stability and Structure of Copper Oxide Surfaces: A First-Principles Investigation. *Phys. Rev. B: Condens. Matter Mater. Phys.* **2007**, *75*, 125420.
(32) Soon, A.; Todorova, M.; Delley, B.; Stampfl, C. Surface Oxides of the Oxygen-Copper System: Precursors to the Bulk Oxide Phase? *Surf. Sci.* **2007**, *601*, 5809−5813.
(33) Therrien, A. J.; Zhang, R.; Lucci, F. R.; Marcinkowski, M. D.; Hensley, A. J. R.; McEwen, J.-S.; Sykes, E. C. H. Structurally Accurate Model for the "29"-Structure of Cu_xO/Cu(111): A DFT and STM Study. *J. Phys. Chem. C* **2016**, *120*, 10879−10886.
(34) Kresse, G.; Hafner, J. Ab Initio Molecular Dynamics for Liquid Metals. *Phys. Rev. B: Condens. Matter Mater. Phys.* **1993**, *47*, 558−561.
(35) Kresse, G.; Furthmüller, J. Efficient Iterative Schemes for *Ab Initio* Total-Energy Calculations using a Plane-Wave Basis Set. *Phys. Rev. B: Condens. Matter Mater. Phys.* **1996**, *54*, 11169−11186.
(36) Kresse, G.; Joubert, D. From Ultrasoft Psuedopotentials to the Projector Augmented-Wave Method. *Phys. Rev. B: Condens. Matter Mater. Phys.* **1999**, *59*, 1758−1775.
(37) Blöchl, P. E. Projector Augmented-Wave Method. *Phys. Rev. B: Condens. Matter Mater. Phys.* **1994**, *50*, 17953−17979.
(38) Perdew, J. P.; Burke, K.; Ernzerhof, M. Generalized Gradient Approximation Made Simple. *Phys. Rev. Lett.* **1996**, *77*, 3865−3868.
(39) Dion, M.; Rydberg, H.; Schröder, E.; Langreth, D. C.; Lundqvist, B. I. Van der Waals Density Functional for General Geometries. *Phys. Rev. Lett.* **2004**, *92*, 246401.
(40) Gunasooriya, G. T. K. K.; van Bavel, A.P.; Kuipers, H. P. C. E.; Saeys, M. CO Adsorption on Cobalt: Prediction of Stable Surface Phase. *Surf. Sci.* **2015**, *642*, L6−L10.
(41) Monkhorst, H. J.; Pack, J. D. Special Points for Brillouin-Zone Integrations. *Phys. Rev. B* **1976**, *13*, 5188−5192.
(42) Methfessel, M.; Paxton, A. T. High-Precision Sampling for Brillouin-Zone Integration in Metals. *Phys. Rev. B: Condens. Matter Mater. Phys.* **1989**, *40*, 3616−3621.
(43) Tersoff, J.; Hamann, D. R. Theory of the Scanning Tunneling Microscope. *Phys. Rev. B: Condens. Matter Mater. Phys.* **1985**, *31*, 805−813.
(44) Tersoff, J.; Hamann, D. R. Theory and Application for the Scanning Tunneling Microscope. *Phys. Rev. Lett.* **1983**, *50*, 1998−2001.
(45) Raval, R.; Parker, S. F.; Pemble, M. E.; Hollins, P.; Pritchard, J.; Chesters, M. A. FT-RAIRS, EELS and LEED Studies of the Adsorption of Carbon Monoxide on Cu(111). *Surf. Sci.* **1988**, *203*, 353−377.
(46) Kneitz, S.; Gemeinhardt, J.; Steinrück, H.-P. A Molecular Beam Study of the Adsorption Dynamics of CO on Ru(0001), Cu(111) and a Pseudomorphic Cu Monolayer on Ru(0001). *Surf. Sci.* **1999**, *440*, 307−320.
(47) Bönicke, I.; Kirstein, W.; Spinzig, S.; Thieme, F. CO Adsorption Studies on a Stepped Cu(111) Surface. *Surf. Sci.* **1994**, *313*, 231−238.
(48) Redhead, P. A. Thermal Desorption of Gases. *Vacuum* **1962**, *12*, 203−211.
(49) Campbell, C. T.; Sellers, J. R. V. Enthalpies and Entropies of Adsorption on Well-Defined Oxide Surfaces: Experimental Measurements. *Chem. Rev.* **2013**, *113*, 4106−4135.
(50) Kreuzer, H. J.; Payne, S. Theories of the Adsorption−Desorption Kinetics on Homogeneous Surfaces. In *Equilibria and Dynamics of Gas Adsorption on Heterogeneous Solid Surfaces*; Zgrablich, G., Rudzinski, W., Steele, W. A., Eds.; Elsevier Science: 1997; pp 1−48.
(51) Wellendorff, J.; Silbaugh, T. L.; Garcia-Pintos, D.; Nørskov, J. K.; Bligaard, T.; Studt, F.; Campbell, C. T. A Benchmark Database for Adsorption Bond Energies to Transition Metal Surfaces and Comparison to Selected DFT Functionals. *Surf. Sci.* **2015**, *640*, 36−44.
(52) Getman, R. B.; Xu, Y.; Schneider, W. F. Thermodynamics of Environment-Dependent Oxygen Chemisorption on Pt(111). *J. Phys. Chem. C* **2008**, *112*, 9559−9572.
(53) Schmidt, D. J.; Chen, W.; Wolverton, C.; Schneider, W. F. Performance of Cluster Expansions of Coverage-Dependent Adsorption of Atomic Oxygen on Pt(111). *J. Chem. Theory Comput.* **2012**, *8*, 264−273.
(54) McEwen, J. S.; Eichler, A. Phase Diagram and Adsorption-Desorption Kinetics of CO on Ru(0001) from First Principles. *J. Chem. Phys.* **2007**, *126*, 094701.

DOI: 10.1021/acs.jpcc.6b07670
J. Phys. Chem. C 2016, 120, 25387−25394